Letters on Materials 15 (4), 2025 pp. 416-422 www.lettersonmaterials.com

Received 28 August 2025; Accepted 23 November 2025 https://elibrary.ru/wnwgeg
https://doi.org/10.48612/letters/2025-4-416-422

Microstructure and micromechanism of fracture of Ni-Al-Cr alloy produced by dual-wire electron-beam additive manufacturing

E. G. Astafurova†, D. O. Astapov, E. A. Zagibalova, S. V. Astafurov,

L. V. Danilova, E. A. Kolubaev

†elena.g.astafurova@ispms.ru

Institute of Strength Physics and Materials Science, Siberian Branch, Russian Academy of Sciences, Tomsk 634055, Russia

Abstract: In this paper, we provide electron microscopic and in-situ X-ray study of microstructure in an Ni-Al-Cr intermetallic alloy that has been obtained by a dual-wire electron beam additive manufacturing using commercial NiCr and Al wires. As-built material possesses a dendritic microstructure that is heterogeneous in both elemental and phase compositions. Different intermetallic phases have been identified with high accuracy using transmission electron microscopy: ordered NiAl-based aluminide with particles of disordered Ni_3Al-based phase in dendritic areas, and mixture of Ni and ordered Ni_3Al phase in interdendrites (all alloyed with Cr). A part of the NiAl-based phase underwent the martensitic transformation B2(NiAl)→$L1_0$ during the additive manufacturing process and post-built cooling. According to in-situ XRD analysis under heating of the alloy up to 1273 K, this transformation has a thermoelastic nature, and the $L1_0$→B2(NiAl) reverse transformation finish temperature is about 873 K. We have noticed the correlation between the phase composition and the tensile fracture micromechanism of the alloy at room temperature: brittle intermetallic B2-NiAl, $L1_0$-NiAl and Ni_3Al-based phases are responsible for high strength but low elongation of the alloy (the tensile strength is 780 MPa and the elongation is 0.2%). An intermetallic alloy is designed to produce intermetallic coatings or to repair bulk intermetallic details using the electron beam additive manufacturing.

Keywords: NiCr alloy, aluminum, intermetallic, electron-beam additive manufacturing, microstructure, fracture

Acknowledgements: *This research was funded by the Government research assignment for Institute of Strength Physics and Materials Science, Siberian Branch of Russian Academy of Sciences, FWRW-2022-0005. Investigations were conducted using equipment of ISPMS SB RAS ("Nanotech" center).*

1. Introduction

Intermetallic alloys are widely used in industry and engineering because of their high chemical and heat resistance. Ni-Al alloys are among the most attractive materials for high-temperature applications [1,2]. Intermetallic Ni_3Al alloy is of particular interest for aviation and space exploration due to a relatively low density and high heat resistance [1–4]. The crystal lattice of Ni_3Al intermetallic compound is an ordered superlattice of the $L1_2$ type. In the unit cell, aluminum atoms occupy corner positions, and nickel atoms — face centers [5]. Unlike steels or pure metals, mechanical properties of Ni_3Al-based alloys increase with increasing temperature and reach a maximum in the range of 873–1273 K. Such abnormal temperature dependence of strength characteristics is associated with a specific mechanism of dislocation movement in the ordered γ'-phase of the Ni_3Al alloy [4,6]. The yield strength (YS) of the Ni_3Al cast alloy at room temperature does not exceed 100 MPa. Thus, its mechanical properties at $T = 297$ K are relatively low [4]. However, the yield strength can reach 500 MPa at $T > 800$ K [9]. Crystallographic texture, solid-solution hardening, and synthesis of a (γ + γ') structure with the optimal value of the mismatch between the crystal lattice constants for γ-Ni and γ'-Ni_3Al phases are among the most valuable strengthening mechanisms of the Ni_3Al alloy [7]. Complex activation of several mechanisms, which can be realized in complex-concentrated intermetallic compounds, looks perspective to create high-strength Ni_3Al-based materials [8,9]. The wide alloying range of the Ni_3Al alloy allows one to use various metals as alloying additives [1,2,4,8–10]. Chromium is a candidate substitution element that provides high solid-solution hardening of the γ-phase and can replace both components in the A_3B compound [10,11].

Owing to the increasing demand for components to be used in high-temperature media, manufacturing of high-performance intermetallic components using conventional processes is limited. The emergence of the additive manufacturing (AM) technology provides new possibilities for solving these issues [12–17]. 3D-printing (or additive manufacturing) is a promising method for producing final products from intermetallic alloys. Additive manufacturing (AM) applies layer-by-layer deposition of raw materials (powder or wire) via their melting using electron or laser energy source [14,17]. In comparison with casting, stamping, and other traditional metal-producing and processing methods, AM allows one to create complex-shaped products of various sizes, including very large objects [13,15,17]. In order to obtain bulk billets with the required phase composition and properties, fundamental research on the mechanisms of their formation is necessary.

Using the wire-feed arc AM, Y. Meng et al. [16] have obtained intermetallic Ni-Al alloy with a gradient Ni-content in the building direction. They reported that the microstructure of the billet changes from a mixture of the NiAl/Ni_3Al intermetallic phases in the lower part of the billet to a more complex composition of $Ni_3Al + \gamma$-Ni/γ'-Ni_3Al in the higher part with the increased Ni concentration. At room temperature, the yield strength and the ultimate tensile stress of the intermetallic compound are 100 and 200 MPa, respectively. Thus, this work has shown the possibility of obtaining intermetallic alloys by additive manufacturing, and properties of the as-built material are typical of the cast Ni_3Al alloy. Based on the data from this work, we successfully obtained the Ni-Cr-Al alloy by electron-beam additive (EBAM) using two commercial wires of NiCr alloy and Al [18]. The AM-fabricated alloy possesses a heterophase structure: a mixture of γ-Ni(Al), Ni_3Al and Ni_3Cr phases has been revealed by scanning electron microscopy (SEM) and X-ray diffraction (XRD) methods. An abnormal temperature dependence of strength properties has been established, and the maximum strength corresponds to a temperature of 873 K (YS = 660 MPa, the ultimate strength exceeds 1000 MPa). Thus, the fundamental possibility of obtaining the Ni_3Al-based material using the EBAM method was demonstrated, and the mechanical properties of this material were close to the properties of conventional Ni_3Al alloys with the ($\gamma + \gamma'$) structure [6,18]. Despite this, the distribution of intermetallic phases and the reasons for low ductility of the alloy in the temperature interval of 300 – 873 K remain unclear.

In this paper we explore the microstructure and phase composition of the EBAM-fabricated Ni-Cr-Al alloy and establish the correlation "fracture mechanism-phase composition" of the alloy at room temperature.

2. Materials and methods

The Ni-Cr-Al alloy was obtained by the method of dual-wire EBAM using an equipment designed at the Institute of Strength Physics and Materials Science (Tomsk, Russia) [17]. The billet had linear dimensions of $30 \times 30 \times 40$ mm^3.

Industrial wires of NiCr and Al (diameter of the wires was 1.2 mm) were simultaneously fed into a melting pool formed by electron beam until 40 layers of the material are deposited on the substrate. The target (calculated) composition of the alloy was 70% Ni-15% Al-15% Cr (mass.%, further related as "3NiCr + Al" alloy). Each layer was formed by applying parallel rows of the material on the substrate. The direction of wire deposition did not change during the AM process. The thickness of each layer was 0.5 – 0.7 mm. The additive manufacturing process was carried out in a vacuum chamber at an accelerating voltage of 30 kV and a beam current of 43 mA. A low-carbon steel plate was used as the substrate. To exclude its influence on the composition of the resulting alloy, five barrier layers of the NiCr alloy were deposited on the substrate before the deposition of the main composition. During the EBAM, chemical homogeneity of the alloy is achieved by mixing the components in the molten pool by an electron beam [14].

For tensile tests, the proportional flat dumbbell-specimens of $12 \times 2.6 \times 1.2$ mm^3 were cut in parallel to the substrate. Specimens were mechanically grinded and polished using silicon oxide suspension. Tension tests were carried out using an LFM 125 (Walter + Bai AG, Switzerland) electromechanical testing system with a high-temperature chamber (300 – 1273 K). The initial strain rate was 5×10^{-4} 1/s

For XRD analysis and electron microscopy, flat specimens were cut in the plane parallel to the substrate. All samples were mechanically ground and polished using silicon oxide suspension. XRD analysis was performed using a DRON-8N X-ray diffractometer (Bourevestnik, St. Petersburg, Russia) equipped with a high temperature vacuum chamber (Cu-K_α radiation). XRD data were collected in the angle interval $2\theta = 40 – 100°$ and the temperature range of 300 – 1273 K. XRD data were analyzed using PowderCell software with the Powder Diffraction File (PDF) database. The microstructure and fracture surface of the specimens were examined using a transmission electron microscope (TEM, a JEOL JEM-2100 microscope operated at an accelerating voltage of 200 kV) and a scanning electron microscope (SEM, a Zeiss LEO EVO 50 microscope equipped with an Energy-Dispersive X-ray Spectroscopy (EDS) system). SEM EDS analysis was used for quantitative evaluation of the base elements (Ni, Al, and Cr) and for qualitative assessment of impurities in the billet (oxygen, carbon, etc.). TEM was equipped with a scanning transmission electron microscope (STEM) unit integrating scanning imaging with transmission analysis [19].

3. Results

Figures 1a, b, and c show SEM images of the microstructure in "3NiCr + Al" alloy. Dendrites and interdendritic regions are clearly distinguished by different SEM contrasts. Since it is impossible to determine which areas were formed first during the EBAM, we will conditionally designate the light grey regions as dendrites (D), and the dark grey are interdendrites (ID). Interdendrites (Fig. 1c) are enriched by Ni and Al, while high concentration of Cr is typical of dendritic regions. The details of the microstructure have been previously described in [18], as they have been revealed by SEM and XRD. We also reported that the anisotropy of mechanical properties in this alloy is suppressed, since the free path of dislocations is not limited by the boundaries of columnar grains characteristic of additively produced samples, but by the interphase boundaries between dendritic and interdendritic regions [18].

Figure 1d shows the results of XRD analysis of "3NiCr + Al" alloy. X-ray analysis confirms SEM EDS data about the phase composition of the material: at room temperature, XRD lines with the highest intensity belong to Ni_3Cr, Ni_3Al intermetallics and Ni. All phases can be additionally alloyed with chemical elements of wires (Al and

Cr). Along with $Ni_3(Al,Cr)$-based intermetallics, X-ray lines can also be attributed to the equiatomic phase of NiAl (B2 or $L1_0$) and pure metals: Al or Cr. However, there are insufficient number of X-ray maxima for analysis of these phases with high accuracy.

Figure 2 shows scanning TEM images and TEM EDS color-coded maps, which show the distribution of the Al, Ni and Cr in the microstructure of the alloy. Images in Figure 2 correspond to the interface between dendritic and interdendritic areas. Nickel is distributed uniformly in the material (Fig. 2 d). Nevertheless, two characteristic regions can be clearly distinguished by elemental composition. The Al-rich interdendritic region is in the upper right part of the images, and dendrite is enriched by chromium (lower left part of the images) (Figs. 2b and c). Despite this, both elements (Al and Cr) are present throughout the specimens. There are Cr-enriched particles, which have round shape (Fig. 2 c). They are located in interdendritic areas and in the interface. Cr-depleted areas are localized in dentritic areas (Fig. 2 c), but complex TEM contrast does not allow one to see them clearly in scanning TEM regime (Fig. 2 a).

TEM bright-field and dark-field images of the microstructure in interdendritic regions are shown in Fig. 3. The main phase is B2-NiAl with ordered BCC crystal lattice (Figs. 3 a and b). Characteristic superlattice reflections are clearly seen in the SAED patterns corresponding to the ordered B2-phase (Figs. 3 b and e). Dark-field images obtained in reflections of B2-NiAl are shown in Figs. 3 c and f: rather homogeneous contrast is typical of these regions, which does not contain any dislocation substructure and subboundaries. In addition to the B2-NiAl phase, the $L1_0$-NiAl martensitic phase with a characteristic micro-twinned microstructure

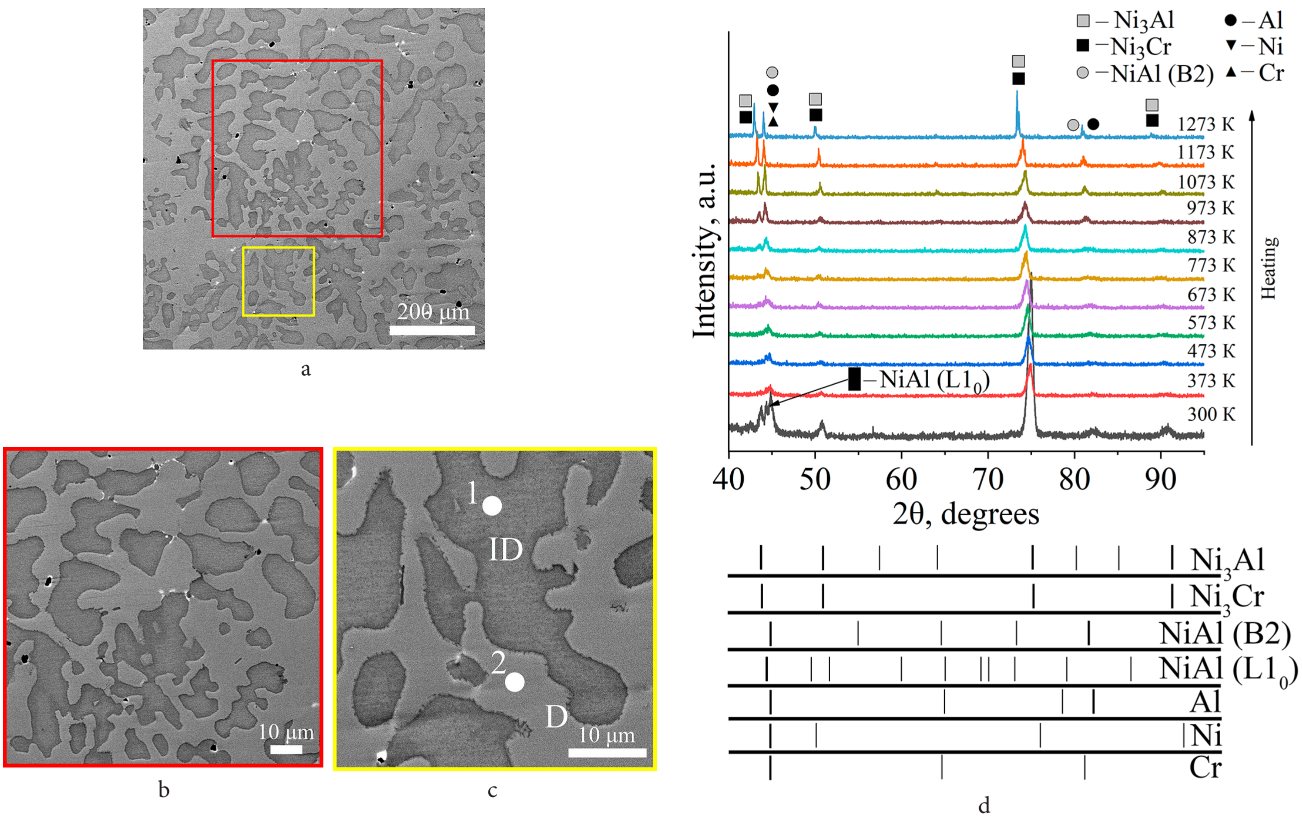

Fig. 1. (Color online) SEM images of the microstructure obtained with different magnifications (a – c), and XRD patterns of "3NiCr + Al" alloy corresponded to different temperatures in the interval from 300 up to 1273 K (d). D — dendrite, ID — interdendrite.

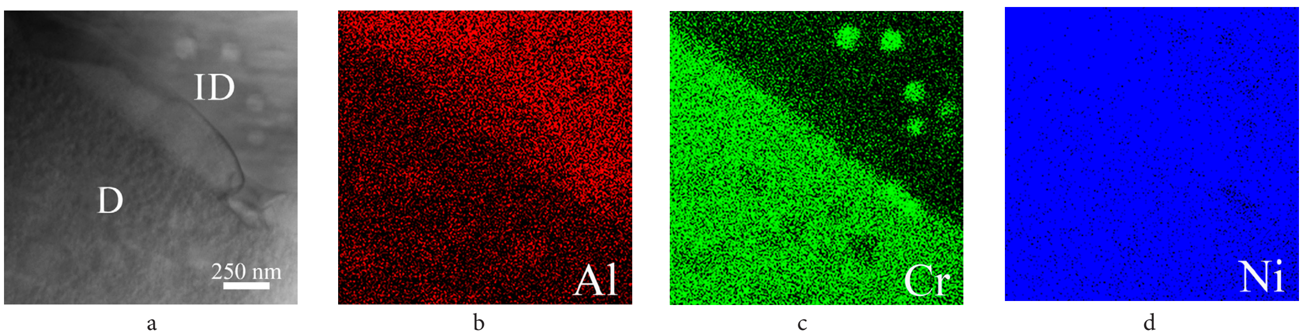

Fig. 2. (Color online) Scanning TEM image (a) and TEM EDS color-coded maps (b – d) showing the microstructure and distribution of the principal elements of the "3NiCr + Al" alloy near the interface "dendrite (D)/interdendrite (ID)": distribution of aluminum (b), chromium (c), nickel (d).

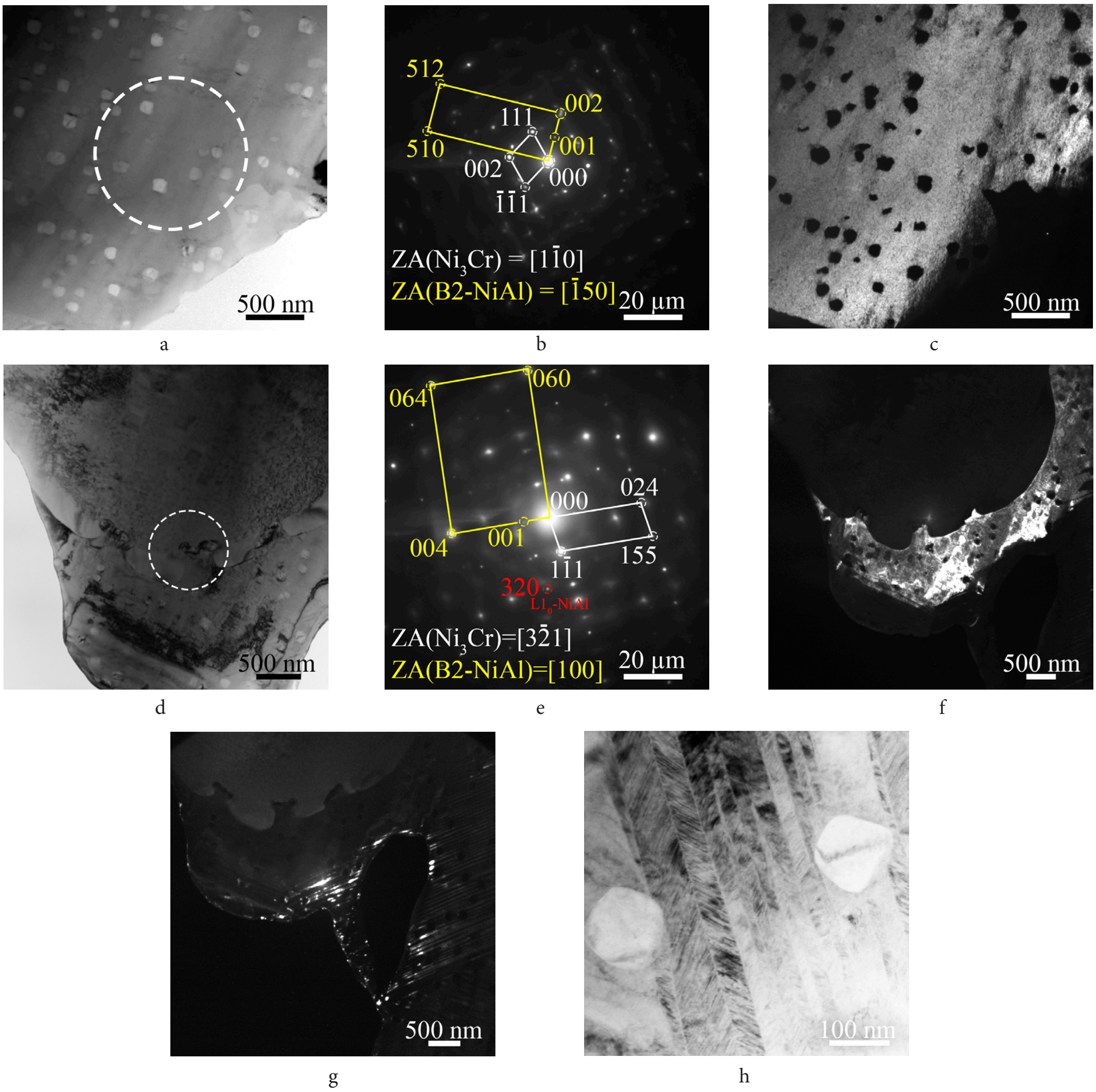

Fig. 3. (Color online) Microstructure of the interdendritic region (a, b, c, h) and boundary between dendritic (lower parts of the images) and interdendritic images (upper parts) (d, e, f, g) in "3NiCr + Al" alloy: bright-field TEM images (a, d, h); dark-field TEM images (c, f); SAED patterns corresponding to the areas circled in Fig. 3 a and d (b and e). Image (c) was obtained in $(001)_{\beta\text{-NiAl}}$ reflection, (f) — in $(001)_{\beta\text{-NiAl}}$ reflection, (g) — in $(320)_{L1_0}$-NiAl reflection.

was found in the interdendritic regions (Figs. 3 d, e, g and h). Large Cr-enriched particles in Fig. 3 c correspond to the intermetallic $Ni_3(Al, Cr)$ phase (Figs. 3 a, b and c). They are spherical in shape and are distributed stochastically.

Thus, interdendrites consist of the B2-phase (NiAl), which is partially transformed to $L1_0$ (NiAl) martensite, and Ni_3Cr intermetallic particles. In contrast to the high-angle boundaries between the dendritic and interdendritic regions, which are clearly visible in TEM images (Fig. 3 d), the interface between the B2 and $L1_0$ phases cannot be easily determined. It is visualized by dark-field TEM analysis or by the appearance of twinned contrast typical of $L1_0$-martensite [20].

TEM images of the microstructure in dendritic regions are presented in Fig. 4. Dendrite is a γ-solid solution (Ni) with particles of the γ'-phase (Ni_3Al-based). γ'-Ni_3Al particles have a typical cuboid form [2–4,7] and are uniformly distributed in dendritic regions. Cuboids are non-uniform in size and shape. That is, there are two structural levels of the γ'-phase: large γ'-phase and fine one. Both types of particles are coherent to the matrix (Figs. 4 b and c). High fraction of the γ'-particles is a result of multiple cooling/heating cycling typical of EBAM process.

The elemental composition of large cuboids (TEM EDS data) is (62-64)%Ni-(12-17)%Cr-(20-24)%Al (at.%). Thus, one can conclude that Cr occupies position of Ni in coarse cuboids, and they are $(Ni, Cr)_3Al$-based intermetallics. The channels of γ-phase between coarse particles contain fine precipitates of Ni_3Al, and their composition is the following: (61-62)%Ni-(26-28)%Cr-(10-11)%Al. Chromium and aluminum can solute in γ-Ni and fine Ni_3Al-based particles, providing solid-solution hardening and assisting high strength of the dendritic regions.

Characteristic SEM images illustrating the fracture surfaces of the EBAM produced alloy after tensile testing at room temperature are shown in Fig. 5. Macroscopically, specimens fracture in a brittle manner, no signs of the neck formation have been noted (Fig. 5a). On the microscale, transgranular brittle and transgranular ductile fractures and intergranular brittle cracking are revealed.

Figure 5c demonstrates a typical brittle transgranular fracture of interdendrites with the NiAl-based microstructure. Cleavage-like patterns are characteristic of them. Fine particles of the Ni_3Al-based phase are seen on the surfaces of cleavages (Fig. 5c). Simultaneously, brittle transgranular regions between cleavages are seen, which correspond to the fracture along interfaces "D/ID" (Fig. 5c). They have a relief inheriting the complex shape of such boundaries observed in SEM and TEM studies (Figs. 1c, 2a and 3d). The traces of ductile transgranular fracture are seen here and there between cleavages (Fig. 5c) at the SEM fracture surfaces, which is due to the high ductility of γ-Ni in interdendritic areas.

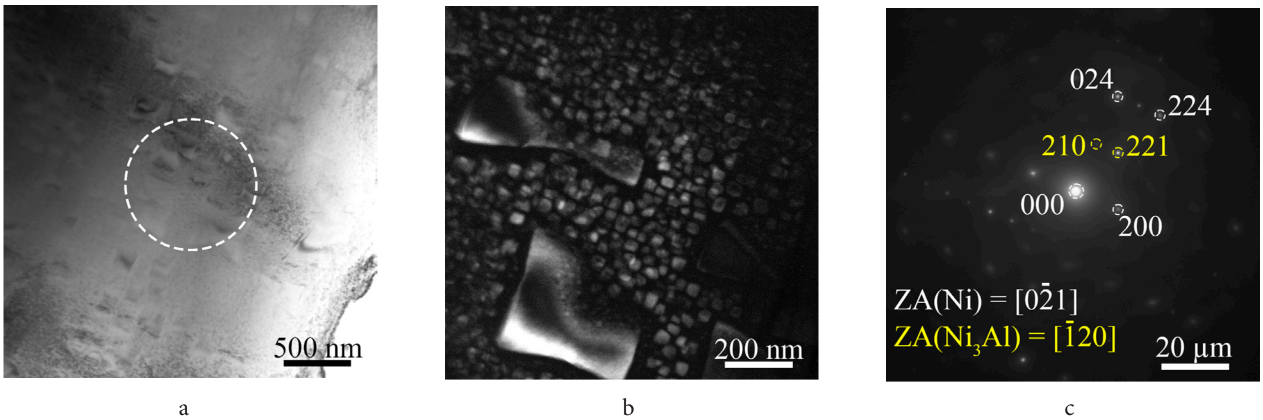

Fig. 4. (Color online) Microstructure of the dendritic area in the "3NiCr + Al" alloy: bright-field TEM image (a); dark-field TEM images obtained in (211) reflection of Ni_3Al phase (b); SAED pattern corresponding to the circled area in Fig. 4a (c).

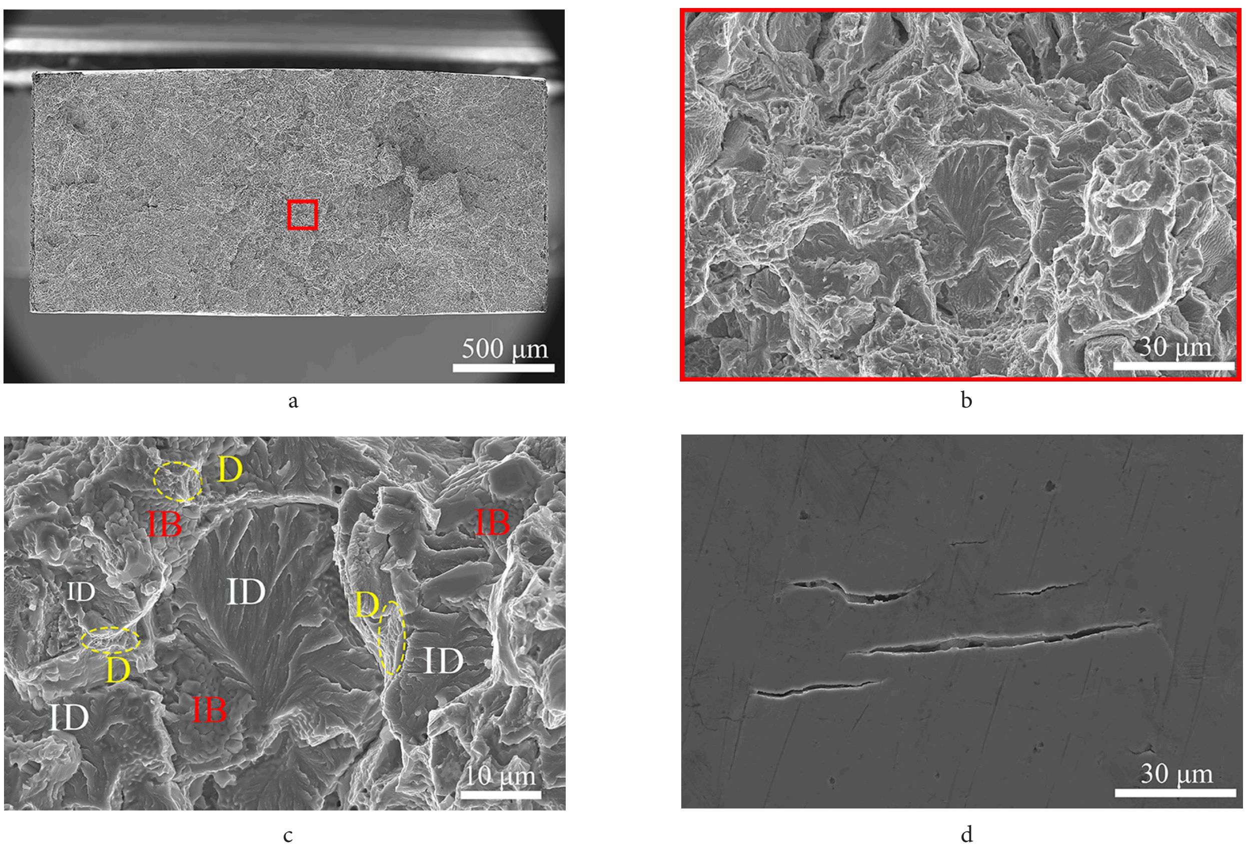

Fig. 5. (Color online) SEM images of the fracture surface (a, b, c) and side surface (d) of the specimen in "3NiCr + Al" alloy after tension at room temperature. Enlarged region of cleavages in interdendrite (ID), failure along interface "dendrite/interdendrite" (IB), and ductile fracture of dendrites (D) (c), microcracks' initiation along IB (d).

4. Discussion

Summarizing the data of TEM analysis, it can be stated that additive manufacturing of Ni-Al-Cr intermetallic alloy based on Ni_3Al phase made it possible to form a complex composite material based on intermetallic compounds. Ordered NiAl-based intermetallic with fine particles of disordered Ni_3Al-based phase forms in interdendritic regions, whereas γ-Ni + ordered γ'-Ni_3Al-based intermetallic (all phases are alloyed with Cr) are typical of dendritic regions. TEM analysis of the microstructure is in accordance with our previous SEM and XRD analysis of the EBAM-fabricated Ni-Al-Cr intermetallic alloy provided in [18].

TEM allows us to reveal that a portion of the B2-NiAl-based phase has undergone a B2-NiAl → $L1_0$-NiAl martensitic transformation during the additive manufacturing process and post-built cooling/heating cycling. This testifies to chemical segregation of the main components of the alloy in dendritic regions, which is one of the disadvantages of the AM processes [14,17]. According to the equilibrium phase diagram for binary Ni-Al alloy, NiAl intermetallic is stable at high temperatures in a rather wide range of Ni concentrations of 45 – 63 at.% [20]. At Ni concentrations higher than 63 at.%, BCC (B2 or β) NiAl intermetallic undergoes martensitic transformation to the $L1_0$ (face centered tetragonal) structure [20 – 22]. According to the TEM EDS data (Table 1, Fig. 2), concentrations of the main components in the B2-NiAl phase are 58% Ni, 3% Cr and 39% Al. Assuming that Cr can occupy the Ni sublattice in a NiAl system, one can conclude that the stoichiometric composition of the interdendritic B2-phase is about $(Ni,Cr)_{61}Al_{39}$. Therefore, the Ni content is close to the concentration limit when the B2 → $L1_0$ martensitic transformation is realized in the binary Ni-Al system. In the case of a ternary alloy Ni-Cr-Al, the martensitic transformation temperatures decrease with increasing Cr-concentrations [22,23], which makes the B2-phase even more stable against martensitic transformations during cooling to room temperature. At the same time, N. V. Kataeva and S. V. Kositsyn with coauthors [21,23] reported that the intermetallic $Ni_{64}Al_{32}Cr_4$ alloy can undergo the B2 → $L1_0$ thermoelastic martensitic transformation in the temperature region 20 – 600°C after annealing at 450°C due to precipitation of Ni-enriched secondary phases (Ni_2Al). Such heating is possible during the EBAM-process. However, this mechanism is not realized according to TEM data (Fig. 3 h).

Instead, TEM EDS analysis also revealed regions in interdendrites with higher concentrations of Ni: (66 – 67)% Ni, 4% Cr, (29 – 30)% Al. These concentrations sufficiently exceed the limit, where B2 → $L1_0$ martensitic transformation is possible in a binary Ni-Al system. So, inhomogeneity of the chemical composition typical of AM-fabricated materials is the primary reason for appearance of $L1_0$ martensite in dendritic regions. *In-situ* XRD analysis (heating of the specimen in diffractometer's chamber with simultaneous recording of the patterns, Fig. 1d) reveals characteristic reflection of $L1_0$-phase at temperatures lower 873 K (600°C), so A_f-temperature is about this value. Thus, interdendritic regions undergo the multiple B2-NiAl ↔ $L1_0$-NiAl martensitic transformation during the EBAM process, which is typically accompanied with accumulation of dislocations, twinning and interphase boundaries [20].

Even though TEM analysis shows that EBAM-fabricated compound includes just a portion of the γ'-Ni_3Al-based phase, this intermetallide is present both in interdendrites (fine precipitates in NiAl) and dendrites (coarse and fine precipitates in Ni). As a result, strength properties and their temperature dependence of the compound, which we previously reported in [18], are typical of γ + (10 – 20)% γ' alloys [21]: YS = 700 MPa, UTS = 780 MPa, El = 0.2% at room temperature. Provided above analysis of the microstructure reveals a correlation between phase composition and fracture micromechanism of the EBAM-fabricated intermetallic compound. Cracks initiate first along interfaces (Fig. 5 d) and then grow into brittle dendritic phase and rather ductile interdendrites. The micromechanisms of fracture in NiAl-based or (γ + γ') compounds are typical of those describe previously elsewhere for Ni-Al intermetallics [24,25]. High volume fraction of brittle B2 and $L1_0$ NiAl-based phases assist brittle fracture of the compound as a whole. To increase the ductility of the EBAM-fabricated material, it was necessary to change the ratio of the main components deposited during EBAM, or to carry out post-built heat treatment of the material to reduce the proportion of the NiAl phase and increase the proportion of the γ + γ' phase.

5. Conclusions

Using advanced SEM, XRD and TEM analysis we provided a deep analysis of the microstructure of the Ni-Cr-Al alloy produced by dual-wire electron-beam additive manufacturing and revealed the reasons for the brittle fracture of the material at room temperature. The following novel results were obtained.

1. As-built material possesses a dendritic microstructure: a mixture of Ni and ordered Ni_3Al phases forms in dendrites, ordered NiAl aluminide with particles of disordered Ni_3Al-based phase is typical of interdendritic regions (all phases are alloyed with Cr).

2. Due to the chemical inhomogeneity, a portion of NiAl-based phase undergoes the B2(NiAl) → $L1_0$ martensitic transformation during the additive manufacturing process. This transformation has a thermoelastic nature, and finish temperature of the reverse $L1_0$ → B2(NiAl) transformation has been determined to be about 873 K.

Table 1. Averaged EDS data for the areas shown in Fig. 2 c and predicted phases according to TEM and XRD analysis.

Spectrum number	Ni, at.%	Cr, at.%	Al, at.%	Phases (TEM)*	Phases (XRD)*
1	61.5	9.9	28.6	NiAl (B2 and $L1_0$)+Ni_3Cr	Ni_3Al, Ni_3Cr, Ni, NiAl($L1_0$), NiAl(B2)
2	61.9	27.2	10.9	Ni+Ni_3Al	

*Phases contain all principal elements of the alloy (Ni, Cr, Al).

3. Brittle fracture and low ductility of the alloy at room temperature is associated with brittle failure of interfaces “dendrite/interdendrite” and intermetallic B2-NiAl, $L1_0$-NiAl phases. Crack initiate at the interphase boundaries “dendrite/interdendrite”.

References

1. R.C. Reed. The superalloys: Fundamentals and Applications. Cambridge University Press (2006) 372 p.
2. T.S. Chester, S.S. Norman, C.H. William, Superalloys II: High-Temperature Materials for Aerospace and Industrial Power, Wiley, 1987, 640 p.
3. Y. Wu, Ch. Li, Y. Li, J. Wu, X. Xia, Y. Liu, Effects of heat treatment on the microstructure and mechanical properties of Ni_3Al-based superalloys: A review, Int. J. Miner. Metall. Mater. 28 (2021) 553 – 566.
4. A.A. Drozdov, K.B. Povarova, O.A. Bazyleva, A.V. Antonova, M.A. Bulakhtina, N.A. Alad’ev, A.E. Morozov, I.S. Pavlov, Intermetallic alloys based on γ'-Ni_3Al: Part I. Features of the structure, formation of (γ'+γ) structures and alloying, Inorg. Mater. Appl. Res. 15 (2023) 235 – 250.
5. T. Zhao, W.Y. Wang, Y. Zhao, P. Li, Y. Zhang, S. Yang, J. Li, Revealing sulfur- and phosphorus-induced embrittlement and local structural phase transformation of superlattice intrinsic stacking faults in $L1_2$-Ni_3Al, J. Mater. Sci. 57 (2022) 12483 –12496.
6. V. Vitek, D.P. Pope, J.L. Bassani, Chapter 51 Anomalous yield behaviour of compounds with LI2 structure, in: F.R. N. Nabarro, M.S. Duesbery (Eds.), Dislocations in Solids, Elsevier, 1996, pp. 135 –185.
7. L. Liu, J. Zhang, Ch. Ai, Nickel-Based Superalloys, in: F.G. Caballero (Ed.), Encyclopedia of Materials: Metals and Alloys, Elsevier, 2022, pp. 294 – 304.
8. V.M. Imayev, Sh.Kh. Mukhtarov, A.V. Logunov, A.A. Ganeev, R.V. Shakhov, R.I. Zainullin, N.Yu. Parkhimovich, R.M. Imayev, Microstructure and mechanical properties of a heat resistant nickel base superalloy heavily alloyed with substitution elements, Letters on Materials 11 (1) (2021) 61– 66.
9. T. Yang, B.X. Cao, T.L. Zhang, Y.L. Zhao, W.H. Liu, H.J. Kong, J.H. Luan, J.J. Kai, W. Kuo, C.T. Liu, Chemically complex intermetallic alloys: A new frontier for innovative structural materials, Materials Today 52 (2022) 161–174.
10. L.B. Ber, S.V. Rogozhkin, A.A. Khomich et al., Distribution of Alloying Element Atoms between γ- and γ'-Phase Particles in a Heat-Resistant Nickel Alloy, Phys. Metals Metallogr. 123 (2022) 163 –177.
11. Z. Mao, C. Booth-Morrison, C.K. Sudbrack, R.D. Noebe, D.N. Seidman, Interfacial free energies, nucleation, and precipitate morphologies in Ni-Al-Cr alloys: Calculations and atom-probe tomographic experiments, Acta Materialia 166 (2019) 702 – 714.
12. C. Chen, T. Cao, C.Xie, S. Xu, Tao Hu, H. Liao, J. Wang, Z. Ren, Recent Progress in Laser Additive Manufacturing of Intermetallic Alloys: Defects, Microstructure, and Mechanical Properties, Additive Manufacturing Frontiers 4 (1) (2025) 200187.
13. K.S. Mukhtarova, R.V. Shakhov, S.K. Mukhtarov, V.V. Smirnov, V.M. Imayev, Microstructure and mechanical properties of the Inconel 718 superalloy manufactured by selective laser melting, Lett. Mater. 9 (4) (2019) 480 – 484.
14. W.E. Frazier, Metal Additive Manufacturing: A Review, J. of Materi. Eng. and Perform. 23 (2014) 1917–1928.
15. E.G. Astafurova, L.V. Danilova, A.S. Nifontov, A.V. Luchin, S.V. Astafurov, E.A. Kolubaev, Intermetallic Fe-Ti alloy obtained by dual-wire electron-beam additive manufacturing, Next Materials 8 (2025) 100739.
16. Y. Meng, J. Li, M. Gao, X. Zeng, Microstructure characteristics of wire arc additive manufactured Ni-Al intermetallic compounds, Journal of Manufacturing Processes 68 (2021) 932 – 939.
17. E.A. Kolubaev, V.E. Rubtsov, A.V. Chumaevsky, E.G. Astafurova, Micro-, Meso- and Macrostructural Design of Bulk Metallic and Polymetallic Materials by Wire-Feed Electron-Beam Additive Manufacturing, Phys. Mesomech. 25 (2022) 479 – 491.
18. E. Astafurova, K. Reunova, E. Zagibalova, D. Astapov, S. Astafurov, E. Kolubaev, Microstructure, Phase Composition, and Mechanical Properties of Intermetallic Ni-Al-Cr Material Produced by Dual-Wire Electron-Beam Additive Manufacturing, Metals 14 (2024) 341– 349.
19. D.B. Williams, C.B. Carter. Transmission electron microscopy: a textbook for materials science, Plenum Press, USA, 1996, 729 p.
20. A.S. Murthy, E. Goo, TEM studies of microtwins in the LI_0 phase in 63.1 at.% NiAl, Acta Metallurgica et Materialia 41 (1993) 3435 – 3443.
21. N.V. Kataeva, S.V. Kositsyn, A.I. Valiullin, Formation of Ni_2Al and Ni_5Al_3 superstructures and reversibility of martensitic transformation in NiAl-based β-alloy, Materials Science and Engineering A 438 – 440 (2006) 312 – 314.
22. R. Kainuma, H. Ohtani, K. Ishida, Effect of alloying elements on martensitic transformation in the binary NiAl(β) phase alloys, Metall. Mater. Trans. A 27 (1996) 2445 – 2453.
23. S.V. Kositsyn, A.I. Valiullin, N.V. Kataeva, I.I. Kositsyna, Investigation of microcrystalline NiAl-based alloys with high-temperature thermoelastic martensitic transformation: I. Resistometry of the Ni-Al and Ni-Al-*X* (*X* = Co, Si, or Cr) alloys, Phys. Metals Metallogr. 102 (2006) 391– 405.
24. M.H. Yoo, S.L. Sass, C.L. Fu, M.J. Mills, D.M. Dimiduk, E.P. George, Deformation and fracture of intermetallics, Acta Metallurgica et Materialia 41 (1993) 987–1002.
25. J. Pelleg, Fracture in B2 intermetallics, in: J. Pelleg (Ed.), Basic Compounds for Superalloys, Elsevier, 2018, pp. 517– 551.